JOURNAL OF CATALYSIS **180,** 270–278 (1998)
ARTICLE NO. CA982280

# The Morphological Evolution of the $MoO_3$(010) Surface during Reactions in Methanol–Air Mixtures

Richard L. Smith and Gregory S. Rohrer[1]

*Department of Materials Science and Engineering, Carnegie Mellon University, Pittsburgh, Pennsylvania 15213-3890*

Received April 14, 1998; revised August 27, 1998; accepted September 11, 1998

**Atomic force microscopy has been used to characterize the evolution of $MoO_3$(010) growth and cleavage surfaces during reactions with air–$N_2$–MeOH mixtures between 200 and 300°C. At reaction temperatures $\geq$250°C, closed step loops, bounded by undercoordinated surface Mo sites, nucleate and grow as the (010) surface volatilizes in a nearly layer-by-layer fashion. The density and crystallography of the new surface sites depend on the composition of the gas mixture in the reactor. In air-rich environments, the step loops have a rectangular shape and are elongated along ⟨001⟩. At any instant, only the uppermost one or two (010) layers are affected by the process. As the concentration of $O_2$ in the feed is reduced, the shape evolves to elongated triangles oriented along ⟨100⟩ and the loops exist on multiple layers simultaneously. During reactions, the observed linear step edge densities can increase from $1 \times 10^3$/cm to greater than $1.5 \times 10^5$/cm. The potential influence of these undercoordinated surface Mo sites on the reactivity of particles with different aspect ratios is discussed.** 

*Key Words:* **molybdenum trioxide; partial oxidation; surface structure; atomic force microscopy.**

## INTRODUCTION

The partial oxidation of methanol (MeOH) to formaldehyde by $MoO_3$ has been the focus of numerous experimental investigations, and it has been proposed that the reaction is surface structure sensitive (1–6). Previous work has demonstrated that the alcohol chemisorbs dissociatively on the $MoO_3$ surface to produce a surface methoxy and a surface hydroxyl (4–6). The bound methoxy decomposes to yield a second hydrogen atom and a formaldehyde molecule. The rate limiting step in this reaction is thought to be the breaking of the C–H bond during methoxy decomposition (3). In the presence of gas phase $O_2$, the reaction apparently conforms to a redox mechanism of the Mars–van Krevelen type (7); the hydrogen liberated during chemisorption and methoxide decomposition react with lattice oxygen to form water vapor (2). Under steady-state anaerobic conditions, however, formaldehyde is not formed. Instead, methane, higher order products (such as dimethyl ether), and hydrogen are observed (2, 6). Coincident with this change in product distribution is a change in the chemistry and structure of the catalyst. When oxygen is eliminated from the feed, the catalyst begins to intercalate the hydrogen liberated during the chemisorption of the alcohol. In the temperature range 200–400°C, the intercalation reaction leads to the precipitation of a hydrogen molybdenum bronze, $H_xMoO_3$, where $0.23 \leq x \leq 0.4$ (8–10).

The influence of the $MoO_3$ catalyst's surface structure on its reactivity during the oxidation of MeOH is the subject of debate. While it is generally recognized that the active sites for methanol chemisorption and oxidation are undercoordinated surface Mo sites, there is disagreement concerning the crystallography and chemical nature of these sites. It was first proposed by Tatibouët and Germain (1) that the basal (010) facets of $MoO_3$ were responsible for formaldehyde formation while the edge facets were responsible for the formation of higher order products such as dimethyl ether and dimethoxy methane. However, the results of temperature-programmed desorption (TPD) spectroscopy studies by Farneth and co-workers (4, 5) later led to the conclusion that the (010) surface plays a subordinate role in the reaction and that the edge facets are responsible for the formation of all products. The anisotropic atomic structure of $MoO_3$ provides support for this conclusion. If free surfaces are created by breaking the smallest number of bonds, the Mo atoms on (010) surfaces remain fully coordinated while those on lateral facets will have reduced coordination and unsaturated bonds. Chung and co-workers (6) have also cited the importance of undercoordinated surface Mo and have deduced that formaldehyde is formed at terminal oxygen (Mo=O) vacancy sites while higher order products are formed at bridged oxygen (Mo–O–Mo) vacancy sites.

The basis of previous structural arguments have rested on a knowledge of the gross shape of $MoO_3$ catalyst particles, the apparent crystallographic distribution of the catalyst's surface area, and the expected termination of the oxide's

[1] To whom correspondence should be addressed. Fax: 412-268-3113. E-mail: gr20+@andrew.cmu.edu. WWW: http://neon.mems.cmu.edu/rohrer.html.



0021-9517/98 $25.00

crystallographically distinct facets. While this information is valuable, little is known about the morphology and structure of the individual facets of the $MoO_3$ particles. Furthermore, the surface morphology of the catalyst is expected to change during reactions, as stoichiometry compensating defects are continuously created and annihilated. The objective of this paper is to describe the structural evolution of the $MoO_3$(010) surface during reactions with air–$N_2$–MeOH mixtures between 200 and 300°C. Under these conditions, it is known that $MoO_3$ catalyzes the oxidation of methanol to formaldehyde (1–3, 6). In addition to (010) cleavage surfaces, we have also examined the structure and evolution of the (010) growth surfaces of crystallites grown by sublimation. Material produced by this method has previously been used to study structure sensitive reactions (11) and has been demonstrated to selectively catalyze the partial oxidation of methanol under the conditions used in the current work (1). Our results demonstrate that the detailed morphology of the (010) surface changes during the reaction as a result of the continuous nucleation and growth of step loops bounded by undercoordinated surface Mo sites. The exact density and crystallographic orientation of these sites depends on the composition of the reactor feed.

## METHODS

### *(a) $MoO_3$ Sample Preparation*

Large single crystals of $\alpha$-$MoO_3$ were grown by chemical vapor transport (CVT) using a procedure described in detail elsewhere (12, 13). Crystals grown by CVT are platelike with large (010) basal facets and typical dimensions along [100], [001], and [010] of 3, 5, and 1 mm, respectively. Single crystals were also grown by sublimation. Approximately 5 g of $MoO_3$ powder (99.95%, Alfa) was charged into the bottom of an open-ended quartz tube ($d = 3$ cm, $l = 20$ cm). This tube was then positioned in a tube furnace such that the closed (charge) end was at the center of the furnace and the open end extended just outside the furnace. To initiate growth, the charge was heated to 720°C and held at this temperature for 2–4 days. The tube was then removed from the furnace and cooled to room temperature so that the single crystals could be harvested. Crystals grown with this technique are generally needle or planklike and less than 50 $\mu$m thick along [010]. The long [001] axis of the crystals sometimes exceeds 15 mm, and along [100], the crystals' dimensions are typically between 0.25 and 1 mm.

### *(b) Surface Reactions*

The single crystal samples of $MoO_3$ were reacted under a continuous flow of gas at atmospheric pressure in a quartz reaction tube (i.d. = 19 mm, length = 1 m). The tube was heated with a nichrome resistance furnace and the hot zone had a length of 30 cm. The temperature at the center of the hot zone was monitored with a type K thermocouple that was completely enclosed in a glass sheath. During the reaction, the single crystals were held in a silica boat ($l =$ 75 mm, $w = 15$ mm, $d = 9$ mm). The boat was positioned in the hot zone with a magnetic transfer rod consisting of a permanent magnet sealed within a quartz tube ($l = 20$ cm). The boat was attached to the transfer rod with chromel wire.

Prior to reaction, CVT grown samples were cleaved with a razor blade (in the ambient) normal to [010] along [100] to produce a fresh (010) surface. The samples were then placed in the silica boat and loaded into the cool zone of the reaction tube under a flow of an air–$N_2$–MeOH mixture. While the samples were typically loaded immediately after cleavage, exposing them to the ambient for up to one week did not appear to affect the experimental observations. Crystals grown by sublimation were not cleaved prior to reaction. They were simply loaded into the boat in an as-grown state. After the samples were loaded into the reaction tube, the system was purged by alternately evacuating (with an oil free pump) and backfilling three times with the gas mixture of interest. During this process, the hot zone of the reactor was maintained at temperature while the sample remained at room temperature in the cool zone. After allowing the gas mixture to flow for an additional 10 min, the boat was transferred to the hot zone and positioned in contact with the glass sheath of the thermocouple. The crystals were then reacted for a predetermined period of time. After the sample was transferred to the hot zone, the measured temperature initially dropped and then rose to approximately 110% of the setpoint before stabilizing at the reaction temperature. Typically, it took less than 10 min for the temperature to stabilize. The reaction was concluded by transferring the sample back to the cold zone of the reactor and allowing it to cool to room temperature under flowing gas. Control experiments were conducted to determine if the presence of the chromel wire or the initial temperature spike influenced the observations. In these experiments, either the sample was heated to temperature under a flow of air–$N_2$ and then exposed to the MeOH containing reaction mixture or it was manually introduced into the hot zone under a flow of the MeOH mixture. At the conclusion of the reaction period, the sample was removed from the reactor manually and cooled to room temperature in the ambient.

The mixtures of dry air (Matheson) and $N_2$ (prepurified, Matheson) were passed through a column of $CaSO_4$ (Drierite) prior to saturating them in a MeOH (99.9+%, Aldrich) bubbler maintained at 0°C or room temperature ($25 \pm 1$°C). The air : $N_2$ mixtures used in these experiments ranged from 100 : 0 to 2 : 98 (by volume). All of the surface reactions were performed at atmospheric pressure in a 230 $cm^3$/min flow of the feed gas. Additional experiments were also conducted with air–$N_2$ mixtures which were

dried, untreated, or saturated with water at room temperature.

*(c) Atomic Force Microscopy Analysis*

After the reacted sample was cooled to room temperature, it was removed from the reactor, mounted on a steel sample disc with double-sided tape, and immediately transferred to the glove box in which a Digital Instruments Nanoscope atomic force microscope (AFM) is housed and operated. The Ar atmosphere within the box is continuously purified, and the concentrations of $O_2$ and $H_2O$ within the box are less than 5 ppm. The AFM was operated in the contact mode (constant force) using pyramidal $Si_3N_4$ cantilevered tips and forces between 0.1 and 8 nN. During the analysis period (several hours), changes in surface structure were not observed and, in fact, at the detection level afforded by AFM, the surfaces were stable indefinitely at room temperature in the glove box or the ambient. Control experiments, in which the samples were transferred directly to the glove box without exposure to the ambient, have demonstrated that the step configuration is not noticeably affected by the brief exposure to air. While adsorption processes are likely to occur during the ambient exposure, this does not alter the AFM images or the surface microstructure of the samples.

The step edge density in the AFM images was estimated with the aid of the image analysis software, Image SXM, which is a subversion of the public domain analysis program, NIH Image. The step edges in each image were first isolated by applying an edge detection filter. A binary contrast threshold was then applied to the edge-enhanced image so that the edges were black and all other areas were white. By determining the fraction of black pixels in the binary image, one can estimate the total step edge length per unit area. All of the linear step densities cited in this paper are in units of the length of a half unit (6.93 Å) step per unit area of the (010) surface. Considering the atomic structure of orthorhombic $MoO_3$ and assuming that steps are formed by breaking the fewest number of bonds (13), we can obtain the approximate area density of unsaturated surface Mo sites by multiplying by a factor of $2.5 \times 10^7$ Mo/cm. However, since the quantity that we actually measure in our experiments is the linear density of half unit step edges, we will refer only to this number in our discussion of the results.

*(d) Gravimetric Measurements*

Parallel experiments were conducted on powdered $MoO_3$ samples to assess any mass changes that might occur during the reactions. Prior to use, the $MoO_3$ powder was calcined in air at 400°C for 24 h and then gently ground in an alumina mortar to break up any powder aggregates. Approximately 0.0350 g of the powder was loaded into a small, dry, porcelain boat which was weighed just before (mass = 0.8670 g) and after loading. The loaded boat was then placed into the quartz reaction tube where it was subjected to a flowing air–$N_2$–MeOH or air–$N_2$–$H_2O$ mixture at 300°C for 10 to 48 h. In all cases, the MeOH or $H_2O$ was introduced by passing the air–$N_2$ mixture through a bubbler at room temperature. At the conclusion of the treatment, the boat was removed from the reaction tube and weighed. As a check, the boat was cleaned, dried, and reweighed at the conclusion of each experiment to ensure that its mass had not changed by more than $\pm 0.0002$ g during the course of the experiment.

*(e) X-Ray Diffraction*

All X-ray data were recorded in the ambient on a Rigaku $\theta$-$2\theta$ powder diffractometer using a step size of 0.05° in $2\theta$ and Cu$K\alpha$ radiation generated by a source operated at 35 kV and 25 mA. In most cases, only small quantities of powder were available. Therefore, samples were mounted by sprinkling the powder onto a glass slide which was coated with double-sided tape.

## RESULTS

*(a) The Structure of the $MoO_3$(010) Surface*

The morphology of the $MoO_3$(010) surface depends on the method of preparation. The fresh cleaved surfaces of CVT grown samples are composed of atomically flat terraces separated by steps which have heights that are an integer multiple of ~7 Å (see Fig. 1a). This characteristic height is half the unit cell repeat length along [010] and corresponds to the distance between the van der Waals gaps which separate the adjacent layers of the structure (6.93 Å). We refer to these features as "half unit" steps. The steps on the cleavage surface are characteristically oriented along [001] and frequently extend unperturbed for distances greater than 100 $\mu$m. The distance between the steps is inhomogeneous and can be as small as a few $\mu$m or larger than 100 $\mu$m.

The morphology of the growth surfaces of the sublimed crystals is governed by the configuration of screw dislocations which act as step sources and facilitate growth (see Fig. 1b). Surfaces formed by this mechanism differ from the cleavage surfaces in two characteristic ways. First, the most frequently encountered steps are integer multiples of the $b$ lattice parameter (~14 Å) rather than $b/2$. This is because only screw dislocations with Burgers vectors equal to an integer multiple of the lattice repeat distance are able to spiral and create new crystal without introducing stacking faults. The second difference is that in addition to the steps along [001], other orientations are frequently observed. This is a natural consequence of growth by the screw dislocation mechanism which leads to significant populations of spiral steps.

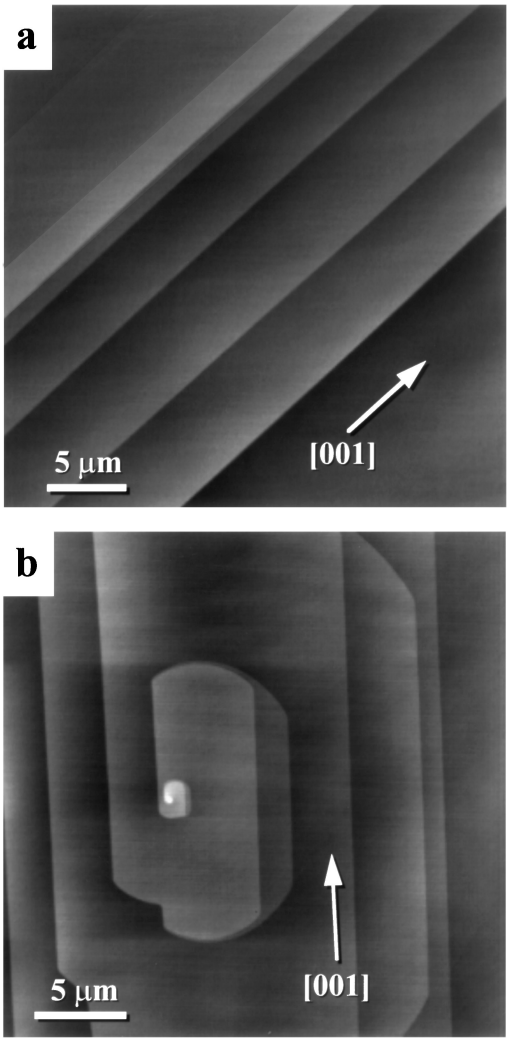


**FIG. 1.** (a) AFM topograph of a $MoO_3$(010) surface produced by cleavage of a CVT grown sample. (b) AFM topograph of a screw dislocation intersecting the (010) growth surface of a $MoO_3$ crystal grown by sublimation in the ambient. The black-to-white contrast in both images is approximately 50 Å. The calculated step edge densities in (a) and (b) are $1.7 \times 10^3$/cm and $2.58 \times 10^3$/cm, respectively.

### *(b) Surface Structure of $MoO_3$(010) during the Partial Oxidation of MeOH*

When $MoO_3$(010) surfaces are reacted with an air–$N_2$–MeOH mixture at 300°C, loops of steps surrounding shallow pits nucleate on the previously flat terraces of the surface. For example, the cleavage surface in Fig. 2a was reacted for 2 h at 300°C in air saturated with MeOH at room temperature. While the lateral dimensions of the pits (darker contrast) can be as large as several micrometers, they are always bounded by half unit steps and are therefore only 7 Å deep. The size of the pits varies from trial to trial but, when all the observations are considered together, it appears that they nucleate as small pits (see Fig. 2a), grow larger, and, eventually, coalesce (Fig. 2b), leaving behind small, irregularly shaped terraces which are one half unit cell in height. As these terraces disappear, new pits nucleate in the next layer. For $O_2$-rich conditions in which the air : $N_2$ ratio was greater than 60 : 40, the differences between the sizes and density of the pits were not noticeably correlated to small differences in the length of the reaction or the exact MeOH content of the feed. For this reason, it appears that we are observing a dynamic process, interrupted at various stages.

The pitting process was observed in all of the air–$N_2$–MeOH mixtures tested with air : $N_2$ ratios between 100 : 0 and 02 : 98. However, the shapes of the pits and their

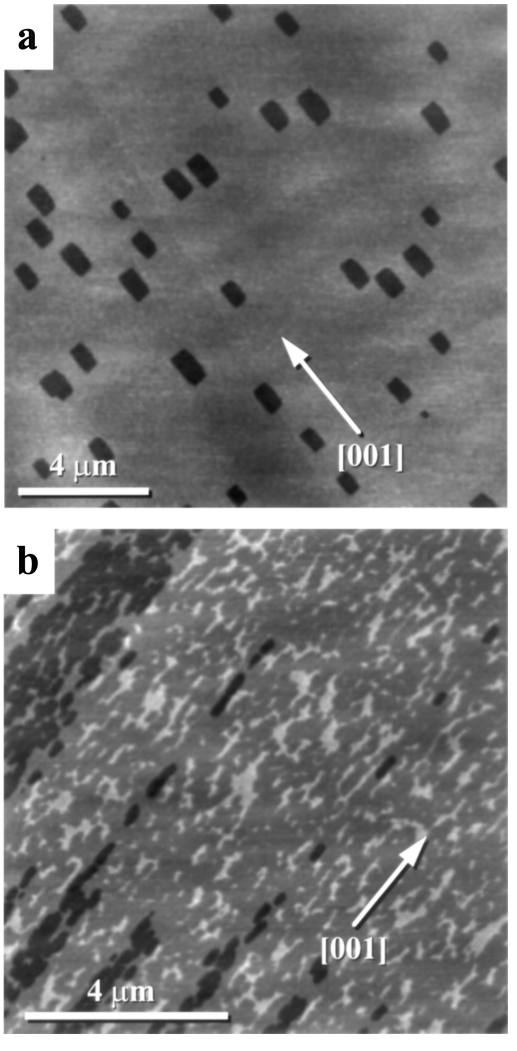


**FIG. 2.** AFM topographs of $MoO_3$(010) surfaces reacted with air–MeOH at 300°C. The surface in (a) was reacted with air saturated with MeOH at 25°C for 2 h and has a step edge density of $4.75 \times 10^3$/cm. The surface in (b) was reacted for 1 h in air saturated with MeOH at 0°C and has a step edge density of $4.6 \times 10^4$/cm. The black-to-white contrast in the images is 40 Å. The residual morphology of the cleavage terraces is evident by the well-defined regions of deeper pits along [001].

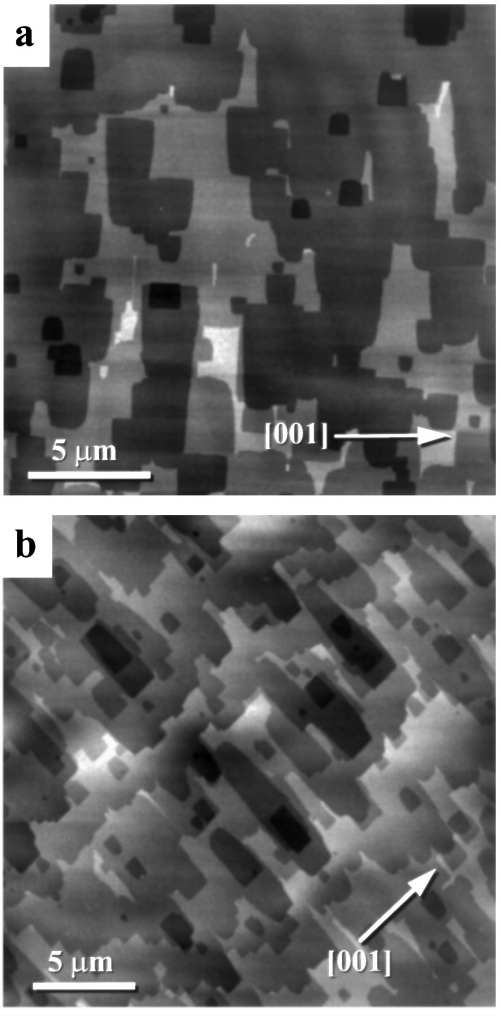


**FIG. 3.** AFM topographs of a $MoO_3(010)$ surface reacted for 2 h at 300°C with a 50 : 50 air : $N_2$ mixture saturated with MeOH at 25°C. The calculated step edge density in (a) and (b) is $7.70 \times 10^3$/cm and $1.04 \times 10^4$/cm, respectively. In (b) there is evidence of [001] step edges from the initial cleavage process. The black-to-white contrast in (a) and (b) is 40 and 60 Å, respectively.

evolution depended on the amount of air in the mixture. Under oxygen-rich conditions, the pits had a rectangular or ovular shape and were always elongated along ⟨001⟩, and only one or two (010) surface layers were exposed at any given time. As the mixture approaches the 50 : 50 concentration, the pits become more equiaxed and are often shaped like a "D" (see Fig. 3). With still lower air concentrations, the pits elongate along ⟨100⟩ and assume a triangular habit. For example, the surface in Fig. 4a was reacted for 1 h at 300°C in a 20 : 80 mixture saturated with MeOH at 0°C. The roughly triangular pits have their long axis oriented along ⟨100⟩. As the air concentration is further decreased, the edges of the triangular pits become straighter and the tips of the triangles become more pointed. The AFM image in Fig. 4b is of a surface reacted for 1 h at 300°C in a 10 : 90 mixture saturated with MeOH at 0°C. Note that on any given layer, all of the triangular pits are oriented in the same manner, with the triangle pointing toward the [100] or [$\bar{1}$00] direction. However, this orientation always reverses as the pits form in the next layer.

A second difference between the higher and lower $O_2$ feeds is that in the lower $O_2$ feeds, pits form and grow simultaneously on more than one surface layer. For example, it is not uncommon to observe pits forming in four or more layers, while only two are affected under the $O_2$ rich (air : $N_2 > 50 : 50$) conditions. This effect can also be seen by increasing the MeOH concentration while maintaining a constant air : $N_2$ ratio. For example, the surfaces in Figs. 5a

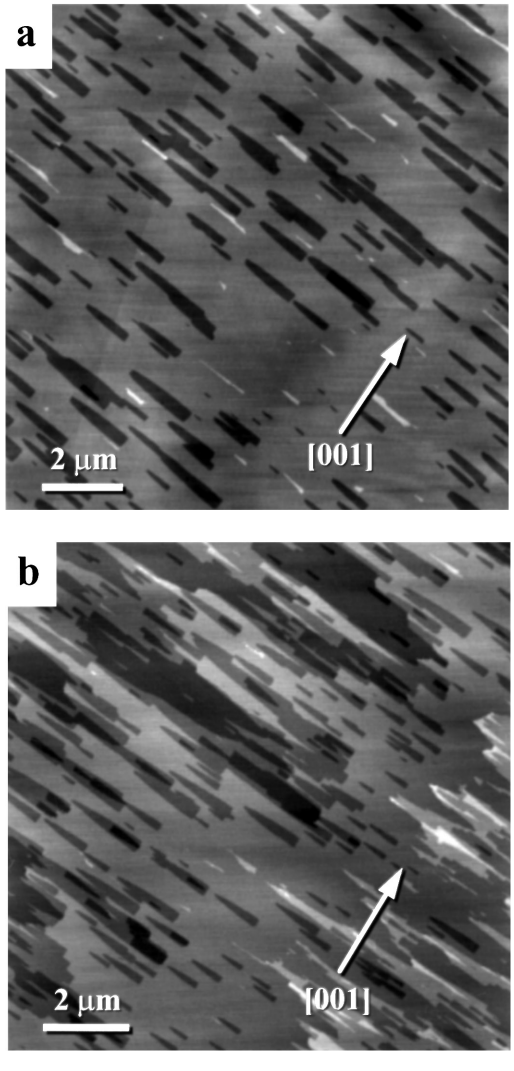


**FIG. 4.** AFM topographs of $MoO_3(010)$ surfaces reacted for 1 h at 300°C in 20 : 80 (a) and 10 : 90 (b) air : $N_2$ mixtures saturated with MeOH at 0°C. The calculated step edge densities in (a) and (b) are $2.14 \times 10^4$/cm and $3.52 \times 10^4$/cm, respectively. The black-to-white contrast is 35 Å (a) and 50 Å (b).

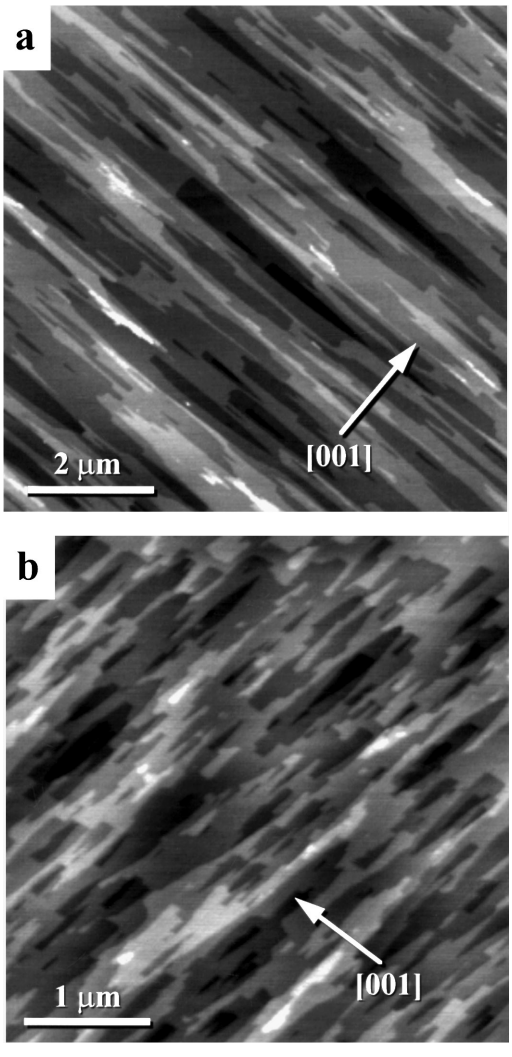


**FIG. 5.** AFM topographs of $MoO_3$(010) surfaces reacted for 2 h at 300°C in 30 : 70 (a) and 10 : 90 (b) air : $N_2$ mixtures saturated with MeOH at 25°C. The calculated step edge densities in (a) and (b) are $6.10 \times 10^4$/cm and $1.51 \times 10^5$/cm, respectively. The black-to-white contrast in the images is 50 Å.

and 5b were reacted in 30 : 70 and 10 : 90 mixtures, respectively, saturated with MeOH at room temperature for 2 h at 300°C. Comparison of Figs. 5b and 4b shows that more layers are affected and higher step edge densities (note the difference in the lateral scale) are realized when the MeOH to air ratio is higher. Surfaces reacted in 02 : 98 (air : $N_2$) mixtures saturated with MeOH at room temperature are roughened to the extent that individual steps are difficult to resolve with AFM. When air is completely eliminated from the feed, $H_xMoO_3$ precipitates form, as described in an earlier paper (10).

We also note that at lower oxygen concentrations, the single crystals sometimes begin to change color. In particular, traces of blue are observed near (001) faces after approximately 2 h at 300°C. This color is similar to that observed when $H_xMoO_3$ precipitates form in crystals treated in MeOH saturated $N_2$ without oxygen. However, based on AFM analysis of the blue regions, there is no evidence for the formation of $H_xMoO_3$ as long as some $O_2$ remains in the feed. Therefore, we assume that the color change is associated with the formation of isolated point defects.

In some regions of the crystal, the pitting process is greatly accelerated. Within 3 h of reaction at 300°C in any of the air–$N_2$–MeOH mixtures, large, isolated etch pits can easily be seen with the aid of an optical microscope. These pits generally have the same habit as the shallow 7 Å pits, but the spiraling structure of the steps around them leads us to believe that they are dislocation etch pits. The fact that they form in the equivalent surface regions on two halves of the same cleaved crystal also supports the conclusion that they are associated with line defects. Because the dislocation etch pit density was inhomogeneous and varied from crystal to crystal, it is difficult to quantify. However, measurements of cleaved CVT crystals yielded an average value of $1.5 \times 10^4/cm^2$. The etch pits continually enlarged with extended reaction times. After 3 h in 100 : 0 mixtures, the pits are approximately 200 nm deep and equiaxed with edge lengths of 6 $\mu$m. In air lean conditions, the pits are up to 80 nm deep and rectangular in shape with edges that are 5 $\mu$m × 1 $\mu$m.

Several experiments were conducted to test the effect of temperature on the process and to see if pitting can be initiated without MeOH. While shallow pits still formed on $MoO_3$(010) surfaces reacted in air–$N_2$–MeOH mixtures at 250°C, pits were not observed after comparable treatments at 200°C. When MeOH is eliminated from the feed and the $MoO_3$(010) surfaces are reacted in an air–$N_2$ mixture between 200 and 300°C, the surface structure is not modified in any manner detectable with AFM. Surfaces reacted with dry or water saturated air, $N_2$, and air–$N_2$ mixtures for as long as 6 h could not be distinguished from virgin surfaces. Therefore, below 300°C, the pitting process is connected to the reaction with methanol. Finally, we note that when subjected to the same reaction conditions, the growth surfaces of sublimed crystals and the cleavage surfaces of CVT grown samples evolved in an identical manner.

### *(c) Weight Loss during the Reactions*

The observations reported above indicate that the $MoO_3$(010) surface is eroding or decomposing in an almost layer-by-layer fashion during reactions with air–$N_2$–MeOH mixtures. There are two possible limiting cases for the fate of the $MoO_3$ removed from the surface during the nucleation and growth of the surface pits: it might volatilize and be carried away in the flowing gas or it may be transported to other regions (perhaps the side facets) of the crystal. These two scenarios are easy to distinguish. In the first case, the sample loses mass and in the second case, the mass will remain constant.

Simple observations favor the first interpretation. After many crystals were reacted in the air–$N_2$–MeOH mixture for 3 h, a blue film accumulated on the thermocouple sheath and the relatively cool walls of the reaction tube where the gas exits the furnace. Because we estimated that the mass lost from any given crystal in a reasonable amount of time was negligible, we conducted a number of experiments on powder samples. In a typical experiment, powdered samples reacted with air saturated with MeOH at room temperature experienced a weight loss of approximately 20% over a 15 h period at 300°C. For example, a 0.0367 g sample reacted in a 100 $cm^3$/min flow of air–MeOH at 300°C for 16.1 h weighed 0.0076 g less at the conclusion of the treatment. Although the powder changed from yellow-white to light green-blue during the reaction, X-ray diffraction confirmed that the samples were phase pure $MoO_3$. While the color change probably indicates a small amount of reduction during the experiment, the weight loss associated with the formation of isolated oxygen vacancies cannot account for a significant fraction of the lost mass.

The blue film at the reactor exhaust accumulated more rapidly during the experiments on powders than during the experiments on single crystals. In one case, the film was collected and analyzed with scanning electron microscopy, energy dispersive X-ray (EDX) analysis, and X-ray diffraction (XRD). The deposit was composed of platelike particles which had dimensions ranging from less than 1 $\mu$m up to 5 $\mu$m. EDX analysis revealed only Mo and O in the deposit. Powder XRD patterns had peaks with *d*-spacings (in Å) of 7.41, 4.76, 3.85, 3.78, 3.22, 3.11, 2.31, and 1.85. The peak at 7.41 Å was intense and well developed, while all the others had relative intensities of less than 15%. Inspection of all the available XRD patterns of Mo–O phases in the JCPDS-ICDD file revealed that the deposit was $Mo_2O_5(OCH_3)_2$ (14). When exposed to UV light, heat, or X-ray radiation, this phase is known to decompose to yield formaldehyde and a blue amorphous hydrogen bronze; one of our samples, exposed to the laboratory ambient for several days, was found to be X-ray amorphous.

Gravimetry experiments at lower air concentrations gave mass losses which were comparable to those experienced in the air–MeOH mixtures at 300°C. However, for mixtures with air : $N_2$ ratios $\leq$ 50 : 50, the interpretation is complicated by the fact that the powder is not completely phase pure at the conclusion of the reaction. The XRD patterns from samples treated in 50 : 50 and 30 : 70 mixtures each included peaks characteristic of $MoO_2$. Based on the relative intensities, the amount of material transformed to $MoO_2$ in the 30 : 70 sample was greater than in the 50 : 50 sample. Mo metal was never detected in any of the patterns. However, even if the entire sample were reduced to $MoO_2$ during the treatment, the mass would decrease only by 11%, approximately half of the total mass lost. Therefore, some portion of the mass loss must still be due to the volatilization process. Finally, control experiments, conducted with dry and water saturated air–$N_2$ mixtures without MeOH, displayed no detectable mass losses over periods as long as 48 h at 300°C.

## DISCUSSION

The results of our AFM and weight loss experiments clearly demonstrate that during the partial oxidation of MeOH, volatilization leads to changes in the morphology of the $MoO_3$(010) surface. For MeOH containing air : $N_2$ mixtures with ratios between 100 : 0 and 05 : 95, 7 Å deep pits nucleate and grow on the (010) surface such that it evaporates in an almost layer-by-layer fashion. At high oxygen partial pressures, only the first one or two (010) layers of the structure appear to be affected, while at lower oxygen pressures, more than five surface layers may be exposed simultaneously. The types of sites exposed along the edges of the pits are influenced by the composition of the gas phase. In $O_2$-rich environments, the steps are generally oriented along ⟨001⟩, while in lower oxygen partial pressures, step edge orientations closer to ⟨100⟩ are favored. As a result of this process, new undercoordinated surface Mo sites, which would not be found on an ideally flat (010) surface, are continuously created during the oxidation reaction.

The volatility of $MoO_3$ is enhanced by the presence of atmospheric water impurities, and the process is linked to the formation and evaporation of volatile oxide–hydroxides, such as $MoO_2(OH)_2$ (g) (15, 16). Above 400°C, $MoO_3$ is known to volatilize in both oxidizing and reducing atmospheres containing water vapor (12). The results presented here demonstrate that at temperatures of 300°C or less, volatilization does not occur at any measurable rate, even in flowing gases saturated with $H_2O$. However, when MeOH is added to the gas stream in this same temperature range, $MoO_3$ volatilizes and a Mo–oxide–methoxide compound, $Mo_2O_5(OCH_3)_2$, is deposited in the cooler exhaust region of the reaction tube.

Based on the generally accepted mechanism of MeOH oxidation on $MoO_3$, we can propose two possible evaporation pathways. The first step of the oxidation reaction is the dissociative chemisorption of MeOH which results in the formation of a surface methoxy and a surface hydroxyl. At this point, if a molybdenum oxide hydroxide molecule desorbs, then the volatilization process is similar to what occurs at higher temperatures in the presence of water vapor. However, in this case, the hydrogen for the process comes from the MeOH rather than from water. The molybdenum oxy-hydroxide might then react with gas phase MeOH during transport or after condensation to form the observed $Mo_2O_5(OCH_3)_2$ deposit at the reactor exhaust. A second and perhaps more plausible explanation is that the surface methoxides which form during the dissociative chemisorption are capable of desorbing as molybdenum

oxide–methoxide molecules, which then condense to form crystalline $Mo_2O_5(OCH_3)_2$ at the reactor exhaust. In either case, the desorption of the volatile molecule leads to the loss of Mo and O from the crystal and results in the growth of surface pits. While both mechanisms are viable, our results do not allow us to distinguish between them. Finally, it should be noted that our weight loss data represent the minimum quantity of material that evaporated from the powder bed; any material which recondensed within the powder bed does not contribute to the total weight loss.

Previous work indicates that MeOH chemisorption occurs at undercoordinated surface Mo sites, which occur at surface oxygen vacancies, at step edges on the basal surface, and on lateral (*h*0*l*)-type facets of the crystal (17). It is tempting to speculate that the pits initially nucleate at or very near undercoordinated Mo sites. The observation that more surface layers are affected in lower oxygen partial pressures supports the idea that the pits nucleate at oxygen vacancies on the (010) surface. As the partial pressure of $O_2$ is reduced, the vacancy concentration should increase, allowing more pits to be created. Once a pit is nucleated, it is then free to grow outward since the edges provide additional undercoordinated Mo sites which are active for chemisorption. One interesting aspect of our observations is that they show that the active sites on this surface are not static. As each pit grows and more material is removed, fresh sites, free of reactor contaminants (such as $H_2O$), are revealed.

Existing data on the structure sensitivity of MeOH oxidation by $MoO_3$ are contradictory. Tatibouët and Germain (1) reported that the (010) surface has a high activity and selectivity for formaldehyde, while Farneth and co-workers (4, 5) have shown that at low temperatures, the $MoO_3$(010) surface chemisorbs very little MeOH. The second result was explained using the idea that the absorption sites are undercoordinated surface Mo and that while these sites occur abundantly on (*h*0*l*) surfaces, they can only be found at step edges and oxygen vacancies on the (010) surface. In part, our results are consistent with this explanation. The density of sites on a fresh (010) surface is initially very low (approximately $10^3$/cm) and we do not expect a significant number of new sites to be generated during a few TPD cycles. On the other hand, our results also show that for longer experiments approaching a steady state, many new sites can be generated on the basal plane and the density of these sites depends on the experimental conditions. Therefore, it is interesting to consider the conditions under which the population of unsaturated Mo sites at the step edges on the basal facets might rival the population of similar sites on the lateral facets of the crystal.

To estimate the relative importance of these new sites, we can consider the $MoO_3$ catalyst which Tatibouët and Germain (1) found to be most selective for formaldehyde formation. The sample they designated "$S_4$" had average dimensions of $W = 0.045$ cm, $L = 0.214$ cm, and $t = 0.004$ cm, where $W$ is the width along [100], $L$ is the length along [001], and $t$ is the thickness along [010]. If we assume that the lateral (*h*0*l*) faces are composed of stacks of steps, each with a half unit height of $b/2 = 6.93 \times 10^{-8}$ cm, then the total linear density of step edges associated with the lateral facets, per unit area of the basal face, $\rho_{(h0l)}$, can be calculated as the total length of the steps divided by the area of the basal plane.

$$\rho_{(h0l)} = \frac{2t(L + W)}{bLW}. \quad [1]$$

Therefore, the linear density of step edges associated with the side facets on the particles used by Tatibouët and Germain was $1.5 \times 10^6$/cm.

For comparison, we can consider the linear density of sites associated with the basal facet, $\rho_{(010)}$. For an as-grown crystal, such as the one shown in Fig. 1b, $\rho_{(010)}$ is only $2.6 \times 10^3$/cm. This is less than 1% of $\rho_{(h0l)}$ and, therefore, we expect the properties of the particles to be dominated by the lateral facets. However, as the reaction progresses, there are two new observed sources of sites active for chemisorption: those associated with the step loops and those associated with the dislocation etch pits. The image in Fig. 2b illustrates that after extended reaction times in the air–MeOH mixtures, the contribution to $\rho_{(010)}$ from step loops can be as high as $4.6 \times 10^4$/cm or approximately 3% of $\rho_{(h0l)}$. The contribution from the etch pits increases with time (the pits grow continuously) and depends on the dislocation density. Our observations indicate that a typical density is $1.5 \times 10^4$/cm$^2$, so that for a square etch pit with a 6 $\mu$m edge length and a depth of 200 nm that forms in 3 h, the contribution to $\rho_{(010)}$ is $1.5 \times 10^4$/cm. Therefore, under air-rich conditions, the total value of $\rho_{(010)}$ is approximately 4% of $\rho_{(h0l)}$.

On the basis of these estimates, it does not appear that the high reactivity of Tatibouët and Germain's (1) platelike particles can be explained by the presence of new edge sites forming on the basal plane. However, we should allow the possibility that an isolated step on the (010) surface might be different from a site on a lateral facet of the crystal in its geometric configuration, energy, and selectivity for specific products. This idea could be tested by using experimental conditions where the ratio of $\rho_{(010)}/\rho_{(h0l)} \geq 1$. For example, it is possible to increase the linear density of step edges by reducing the concentration of air in the feed, increasing the depth of the pits by higher temperature treatments (12), or by increasing the aspect ratio of the particles. Increasing $\rho_{(010)}$ or decreasing $\rho_{(h0l)}$ by a factor of 10 will make the two quantities comparable. By comparing the reactivity of particles with similar values of $\rho_{(h0l)}$ but different values of $\rho_{(010)}$, it will be possible to determine whether or not the sites on the basal plane behave differently from those on the lateral edges.

As a final note, it should be pointed out that since the $\rho_{(010)}/\rho_{(h0l)}$ ratio depends on the details of the experiment

(time, temperature, gas composition), the results from previous studies of the structure sensitivity of reactions on $MoO_3$ should be applied with caution. In particular, conclusions from experiments of extremely short duration are not expected to hold universally and those based wholly on the macroscopic form of the crystal might not accurately depict the density of active sites.

## ACKNOWLEDGMENT

This work was supported by the National Science Foundation under YIA Grant DMR-9458005.

## REFERENCES

1. Tatibouët, J. M., and Germain, J. E., *J. Catal.* **72**, 375 (1981).
2. Machiels, C. J., and Sleight, A. W., *in* "Proceedings of the 4th International Conference on the Chemistry and Uses of Molybdenum" (H. F. Barry and P. C. H. Mitchell, Eds.), p. 411. Climax Molybdenum Co., Ann Arbor, MI, 1982.
3. Machiels, C. J., and Sleight, A. W., *J. Catal.* **76**, 238 (1982).
4. Farneth, W. E., Ohuchi, F., Staley, R. H., Chowdhry, U., and Sleight, A. W., *J. Phys. Chem*. **89**, 2493 (1985).
5. Farneth, W. E., Staley, R. H., and Sleight, A. W., *J. Am. Chem. Soc.* **108**, 2327 (1986).
6. Chung, J. S., Miranda, R., and Bennett, C. O., *J. Catal.* **114**, 398 (1988).
7. Mars, R., and van Krevelen, D. W., *Chem. Eng. Sci.* **3**, 41 (1954).
8. Vergnon, P., and Tatibouët, J. M., *Bull. Soc. Chim. Fr.* **11**–**12**, 455 (1980).
9. Guidot, J., and Germain, J. E., *React. Kinet. Catal. Lett.* **15**, 389 (1980).
10. Smith, R. L., and Rohrer, G. S., *J. Catal.* **173**, 219 (1998).
11. Bruckman, K., Grabowski, R., Haber, J., Mazurkiewicz, A., Sloczynski, J., and Wiltowski, T., *J. Catal.* **104**, 71 (1987).
12. Smith, R. L., and Rohrer, G. S., *J. Catal.* **163**, 12 (1996).
13. Smith, R. L., and Rohrer, G. S., *J. Solid State Chem*. **124**, 104 (1996).
14. McCarron, E. M. III, Staley, R. H., and Sleight, A. W., *Inorg. Chem*. **23**, 1043 (1984).
15. Millner, T., and Neugebauer, J., *Nature* **163**, 601 (1949).
16. Belton, G. R., and Jordan, A. S., *J. Phys. Chem*. **69**, 2065 (1965).
17. Farneth, W. E., McCarron, E. M. III, Sleight, A. W., and Staley, R. H., *Langmuir* **3**, 217 (1987).